17 December 1982, Volume 218, Number 4578 **SCIENCE**

Advances in Picosecond Spectroscopy

P. M. Rentzepis

Summary. Progress in the technology of picosecond spectroscopy in the past few years has made possible the generation of well-characterized pulses emitted by synchronously pumped tunable dye lasers. In addition, the development of sensitive emission and absorption detection methods and the advent of picosecond Raman and coherent anti-Stokes Raman spectroscopy make possible the direct observation of picosecond transient spectra and lifetimes. The information obtained allows the complete determination of mechanisms through the identification of transient states, radicals, and ions that evolve during the course of a chemical or biological reaction.

Identification of the role of the various molecular species generated in the course of chemical reaction has been the focus of chemical experiment, theory, and speculation since the discovery of atoms and molecules. A vast amount of knowledge has been accumulated, yet in most cases the exact mechanism of even the most simple processes such as dissociation, isomerization, and radical formation has escaped direct experimental observation. Only recently has it been possible to make detailed experimental studies, by means of picosecond absorption, emission, and Raman spectroscopy, on a time scale appropriate for the observation of fundamental chemical steps. Although the final product of most reactions is, of course, known and overall rates of the simplest reactions can be estimated from measurements of quantum yield and radiative lifetime, detailed knowledge of the process, including the electronic state involved, intersystem crossing rates, radical formation, radical lifetime, and torsional rearrangement, cannot be obtained unambiguously without direct experimental evidence.

An illustration of how fundamental chemical processes can be delineated by picosecond spectroscopy is provided by recent experimental work on the dissociation of haloaromatic compounds (*1*, *2*). It is known that haloaromatics dissociate to the parent aromatic radical and the halogen after excitation with light of the appropriate wavelength. The course of events that leads to dissociation after population of the allowed excited states was unknown until recently. Indirect experimental data suggest that dissociation takes place directly from the singlet state, yet other indirect experimental data indicate that crossing to the triplet state precedes dissociation. For small molecules such as CO_2, HCN, and ICN, theoretical predictions (*3*) are in fair agreement with the fluorescence data on vibrational state distributions. However, large polyatomic molecules such as the haloaryls are characterized by dense vibrational manifolds, which provide for dissipation of the absorbed photon energy through internal conversion and intersystem crossing. These processes may compete favorably with direct photodissociation of the molecules and cause predissociation to become the dominant process. Molecular beam studies by Bersohn and co-workers (*4*) showed that photofragment formation in haloaryls may be caused by either (i) direct dissociation from an upper electronic state or (ii) internal conversion to a lower excited state, followed by intersystem crossing to a low-lying triplet state and thence into a dissociating $^3(\pi,\sigma^*)$ level associated with the carbon-halogen (C–X) bond. However, intersystem crossing might also lead by internal conversion to lower energy triplets and, conceivably, relaxation to the ground state by radiative or radiationless transitions.

In view of the dense vibrational manifolds of large molecules, the dissociative channel that is operative with high efficiency may not be predictable with certainty for various levels of photon excitation. Neither can a single type of measurement—whether it be quenching of triplet states or radicals with reactive species, or fluorescence or quantum yield measurements—provide the data needed to directly identify the electronic states involved and the rates that govern their population and depletion. Because of the inherent limitation of each technique and the fact that many relaxation rates are in the range 10^9 to 10^{12} sec^{-1}, we have simultaneously employed fluorescence and absorption picosecond spectroscopy to identify the mechanism and transient states. The fluorescence spectrum alone provides a means of identifying the emitting upper electronic level and determining its lifetime, which establishes the rate of its decay, but it gives no information about radiationless energy dissipation or the state from which the energy is dissipated. However, by combining fluorescence information with time-resolved absorption spectra of the ground state, showing its depletion and repopulation, and spectra of all the transient states and species, a direct measurement of the rates of formation and decay is obtained that provides a unique and complete histogram of the evolution of a photochemical reaction. The mapping of a chemical reaction may be illustrated by following the avenues that lead to the dissociation of the iodo-, bromo-, and chloroaromatics.

P. M. Rentzepis is head of the Physical and Inorganic Chemistry Department at Bell Laboratories, Murray Hill, New Jersey 07974.

0036-8075/82/1217-1183$01.00/0

The known electronic spectra of the particular haloaromatics under study here show that halonaphthalenes and haloanthracenes can be excited by either the fourth harmonic, 266 nanometers, or third harmonic, 355 nanometers, of a neodymium/yttrium-aluminum-garnet (Nd^{3+}/YAG) laser. For these photon energies, the molecule is excited with a few thousand wave numbers of excess vibrational energy. The relaxation rate to the thermalized singlet was determined to be less than 5 picoseconds by two independent measurements, showing (i) the absence of unrelaxed fluorescence and (ii) the fact that the relaxed fluorescence (vibrational quantum number $\nu = 0$) rise time was also found to be completed within 5 psec. The processes that are candidates for dissipation of the S_1 (first excited singlet state) population may be described as (i) radiative decay to the ground state, $S_0 \leftarrow S_1$; (ii) direct dissociation from S_1; (iii) intersystem crossing to an upper vibronic state of a triplet level; and (iv) nonradiative decay to S_0.

In the case of intersystem crossing it is expected that relaxation to the lowest vibronic level of T_1 (the first excited triplet state) will be fast since vibrational deactivation, $T_1^n \rightarrow T_1^0$, in liquid solutions has been shown to occur with a rate of $\sim 10^{12}$ sec^{-1} (*5*). As in the case of the singlet state, three channels may be open for the deactivation of the triplet: (i) phosphorescence to the ground state, $S_0^n \leftarrow T_1^0$; (ii) nonradiative decay to the ground state, $S_0^n \leftarrow T_1^0$; and (iii) predissociation through a $^3(\pi,\sigma)$ state resulting in fragmentation to an aromatic radical and a halogen. There is, of course, a possibility of predissociation directly from the upper singlet π,π^* aromatic states to the C–X singlet π,σ^* states (*6, 7*).

If energy dissipation proceeds through a triplet state, the rate should increase from chloro- to bromo- to iodoaromatics owing to the known increase in spin-orbit coupling as the atomic number of the substituted halogen increases. This is similar to the strong intramolecular perturbations known to occur in chelated organic molecules such as Cu^{2+} and Ni^{2+} porphyrins. The spin-orbit coupling is manifested in the ground state halogen atom $1S_1$ fine-structure splitting, $^2P_{3/2} \rightarrow {}^2P_{1/2}$. On the basis of this knowledge it would be expected that the singlet-state decay lifetimes of bromo- and iodoaromatics would vary as the square of this coupling. However, as the picosecond data will show, these lifetimes differ by approximately an order of magnitude. Such data suggest that spin-orbit coupling may not be the dominant factor in the energy redistribution process, and thus it is difficult to assign with certainty the mechanism that governs the reaction. Only by obtaining direct kinetic and spectroscopic evidence can the effects of the various parameters such as solvent, heavy atom substitution, temperature, and polarity be unambiguously assigned.

The combined data on time-resolved transient absorption spectra, emission kinetics, and the spectra and formation and decay kinetics of the radicals formed provide, we believe, an unambiguous and perhaps novel means for understanding the mechanisms involved in chemical reactions. The fate of excited molecules is followed directly by identifying and monitoring the evolution and decay of each transient spectroscopic state and species during the process of dissociation and recombination.

Experimental Studies

Several systems for the generation of picosecond pulses have been used, varying from a single-shot Nd^{3+}/glass laser emitting pulses of $\sim$ 8 psec full width at half-maximum (FWHM) to a high-repetition-rate dye laser emitting pulses of $\sim$ 2 psec FWHM. In all cases, the oscillator output is increased by a set of amplifiers, which can increase the output per pulse by a factor of 100 or more. Dye lasers generate shorter pulse widths, but usually with lower energy content, and their repetition rate can be higher. However, amplification by using Nd^{3+}/YAG lasers to pump the dye amplifier normally limits the repetition rate to ≤ 10 hertz. Nevertheless, the shorter pulse width, $\sim$ 2 psec, and the tunability of dye lasers provide very desirable features. Since the Nd^{3+} lasers have been described quite extensively (*8*), I will only briefly describe the synchronously pumped picosecond dye laser that we are currently using. The principal components of the pumping source and ring dye laser were manufactured by Spectra Physics. These consist of a mode-locked argon laser (Fig. 1) that inserts a pump pulse of $\sim$ 100-psec duration into a ring laser. The "argon pulse" transverses the optical path shown in Fig. 1 and excites the dye as it flows through a jet, generating a train of picosecond pulses. The output of the dye laser consists of picosecond pulses with the following characteristics: pulse width, 2 psec; energy, $\sim$ 100 microjoules; and wavelength range, 560 to 800 nm with appropriate dye. The pulses are subsequently amplified in three dye laser amplifiers pumped by the 530-nm second harmonic of Nd^{3+}/YAG lasers. The amplified pulses are frequency doubled, resulting in $\sim$ 0.3-millijoule pulses which are suitable for excitation of molecular species in the ultraviolet region. The output pulse of the dye laser is shown in Fig. 2.

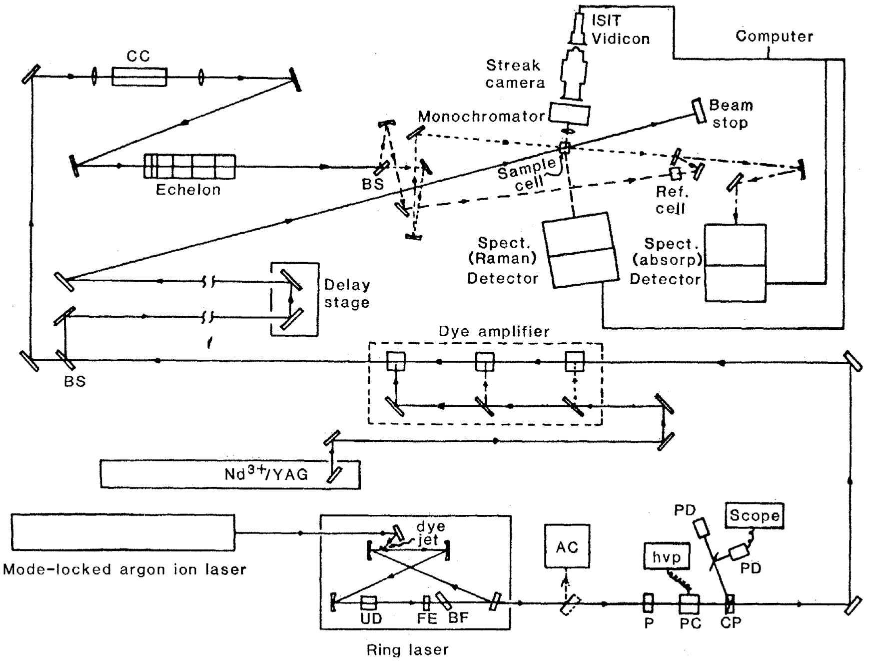

Fig. 1. Experimental arrangement for picosecond absorption emission and Raman spectroscopy. The oscillator consists of a mode-locked argon laser that pumps a ring dye laser. The output is increased by a set of dye amplifiers pumped by Nd^{3+}/YAG lasers. Detection and processing of data are accomplished by use of a streak camera, ISIT (intensified silicon intensified target) vidicon(s), and an optical multichannel analyzer coupled to a dedicated minicomputer. Abbreviations: *CC*, continuum cell; *BS*, beam splitter; *UD*, unidirectional device; *FE*, fine etalon; *BF*, birefringent filter; *AC*, autocorrelator; *PD*, pulse detector; *HvP*, high-voltage pulse source; *PC*, Pockels cell; *CP*, corner prism; *P*, polarizer.

The optical arrangements for absorption and emission spectroscopy are essentially the same; the principal differences are the frequent use of an echelon for the time resolution of the excited state decay, instead of a delay stage, and the generation of a broadband picosecond continuum in a liquid, such as D_2O-H_2O, for transient absorption spectroscopy. Figure 1 is a schematic representation of a complete system capable of monitoring (i) transient absorption spectra from ~ 1 psec to several nanoseconds, (ii) emission spectra and decays, and (iii) picosecond and nanosecond Raman spectra.

Picosecond transient absorption. A picosecond pulse, at 265 nm, excites the sample (*9*); it is followed by a broad continuum pulse that interrogates a region of the spectrum, 300 to 800 nm, at preselected periods of time such as −20, 0, 5, 20, 100, and 500 psec and 5 nsec. Representative transient absorption spectra (*8*) are shown and discussed later in this article. Decay lifetimes in the form of plots of change in absorbance (ΔA) versus time (t) may be recorded by means of an echelon for preselected wavelength ranges. The continuum light is collimated into the sample, so that a region of the sample smaller than that exposed to the excitation pulse is illuminated, and then imaged onto the slit of a 1-meter spectrometer. A two-dimensional vidicon, attached to the exit slit of the spectrometer, collects and transfers transient spectra of decay lifetime curves to an optical multichannel analyzer (OMA). Analysis, averaging, error bar determination, and graphics are performed with an Eclipse Data General computer. Typically, 10 to 20 laser shots with and without excitation are averaged for each spectrum or decay curve, the actual number being determined by the signal-to-noise ratio. In all cases—for absorption, emission, and Raman spectra—care is exercised to ensure that the signals observed are not the result of multiphoton processes or nonlinear or saturation effects. This is achieved by reducing the photon content of the excitation pulse to as low as 20 $\mu J/mm^2$ for investigations of biological materials. In addition, corrections for the temporal dispersion of the continuum light are taken into account when the lifetime computations and spectra fits are performed. The kinetics (ΔA versus t) are evaluated by calculating the areas under each segment of the probe and reference beams for both excitation (ex) and nonexcitation (no ex) shots.

$$\Delta A(\lambda) = \frac{-\log_{10}[a^{\mathrm{ex}}(\lambda)/a_0^{\mathrm{ex}}(\lambda)]}{a^{\mathrm{no\ ex}}(\lambda)/a_0^{\mathrm{no\ ex}}(\lambda)}$$

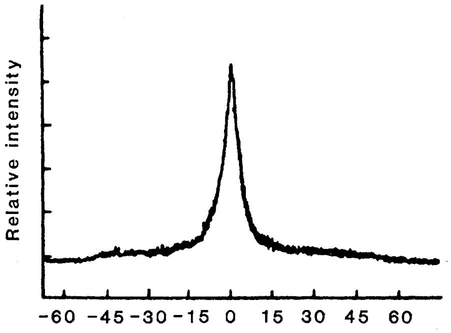

Fig. 2. Typical picosecond pulse emitted by the pulse generation system shown schematically in Fig. 1.

With a two-dimensional vidicon one can record spectra and kinetics simultaneously. Figure 3 illustrates the data and format available from the computer. In addition, a streak camera, which is normally utilized for emission, can be easily used as a detection instrument for absorption.

Transient emission spectra and kinetics. The most useful instrument for recording emission decay is a streak camera that is capable of resolving ~ 2-psec lifetimes and has spectral sensitivity from the deep ultraviolet to near infrared. The emitted light, induced by a picosecond excitation pulse, is collimated by a collection lens. It is then passed through a monochromator, or set of filters, and focused on the slit of the streak camera. The image is amplified by an image intensifier and transferred to an OMA. The decay curve thus obtained must be corrected at each streak rate because of the changes in sensitivity of the streak camera–OMA system with position in the camera plane. A second source of error may arise from the inherent nonlinearity of the time base of the streak camera, which at the fastest time scale (~ 0.8 psec) may vary by about 30 percent across the streak record. These possible errors are eliminated by calibration with a molecule whose spectra and emission decay are well known. This procedure also allows for vignetting in the relay optics and sensitivity variation of the individual OMA channels (*10*). Finally, the true rise time and decay lifetimes of a process are determined by deconvolution of the excitation pulse from the observed fluorescence lifetime. The resulting fluorescence is fit to a rise time, τ_R, and decay time, τ_f. To ascertain reliability in the decay lifetimes, approximately 20 scans are averaged and fitted after correction for instrumental errors. This procedure for the determination of fluorescence lifetimes was used by Barbara *et al.* (*10*) to obtaining the curves of Fig. 4. Transient emission spectra can easily be recorded by means of a monochromator and vidicon. By gating the vidicon to short recording times, we were able to eliminate long-lived fluorescence originating from the parent species or other impurities.

Picosecond Raman spectra. In principle, one can detect and record Raman spectra of transient species within a few picoseconds after excitation. The most common approach utilizes a resonance Raman probe pulse, which takes advantage of the intensity enhancement derived from using a probe frequency near a molecular transition. The system for generating excitation pulses is the same as that used in studying absorption and

Fig. 3. Illustrative three-dimensional display of a picosecond absorption process.

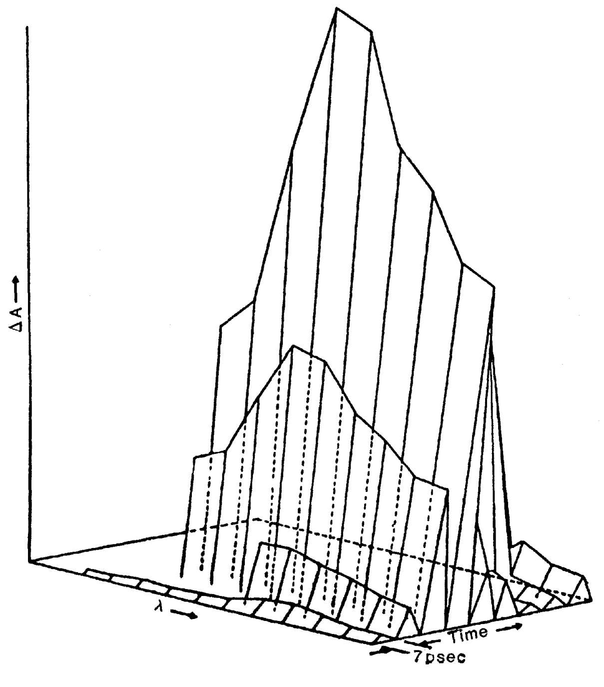

emission spectra; however, a second probe pulse is used to monitor the Raman scattering. This pump-probe technique (*11*) is, in principle, very similar to that used for extended time absorption. The intensity of the Raman spectra generated by a single excitation-probe pulse pair depends in many cases on relatively high-energy excitation pulses, which may result in nonlinear excitation or the denaturation of biological samples. To eliminate the possibility of such effects we use a high repetition rate—that is, a large number of pulses of very low energy generated by a synchronously pumped dye laser. The low energy maintains the excitation in the linear regime, and the high repetition rate makes it possible to average more than 10^3 pulse-probe signals in a short period of time so that a high signal-to-noise ratio is attained. A second quite significant handicap, that of a high background Raman signal from the solvent, can be overcome by using xenon as the solvent. This solvent, as pointed out by D. C. Douglass (*12*), has several advantages: it does not produce Raman scattering, and it can be used in the gas phase or as a liquid (~ 16.6°C) or solid (−118°C). The combination of these improvements makes it possible to generate spontaneous picosecond Raman spectra and eliminates the restriction to resonance probing and the inherent possibility of stimulated fluorescence. Recently, picosecond coherent anti-Stokes Raman spectra have been demonstrated.

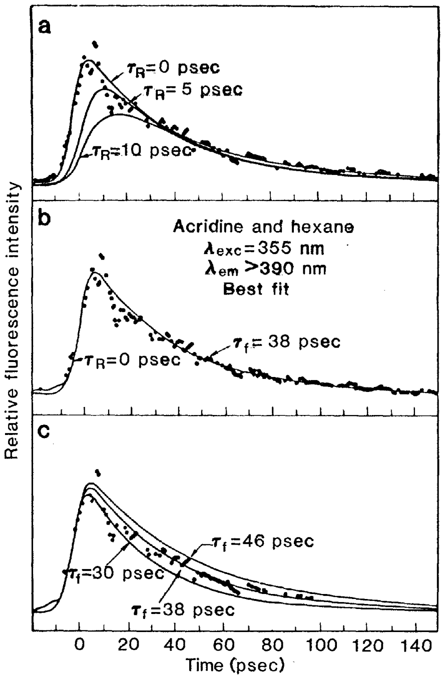

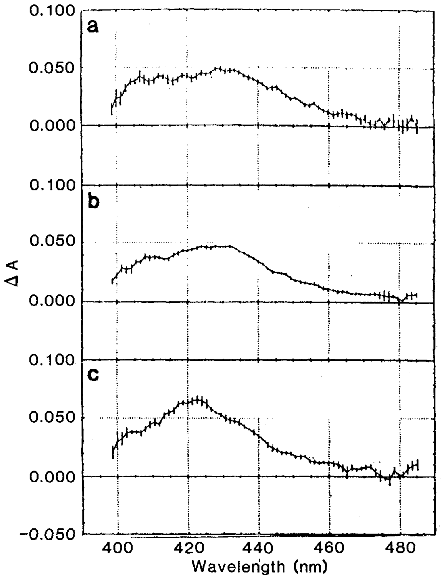

Fig. 4 (left). Emission decay curves of acridine in solution. The dots are the experimental points and the solid lines computer-fitted curves. Fig. 5 (right). Transient picosecond absorption spectra of 1-chloronaphthalene in hexane at 20°C on excitation with a 265-nm picosecond pulse; the spectra were recorded at (a) 25 psec, (b) 100 psec, and (c) 500 psec after excitation.

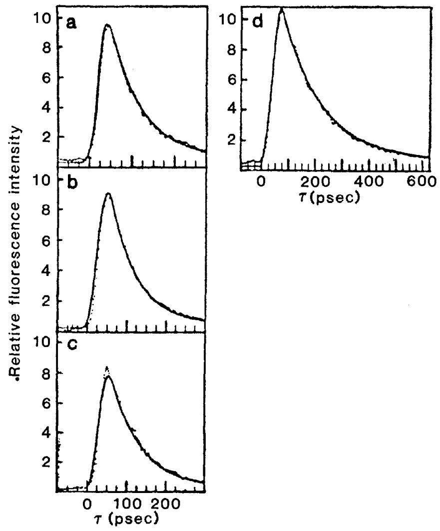

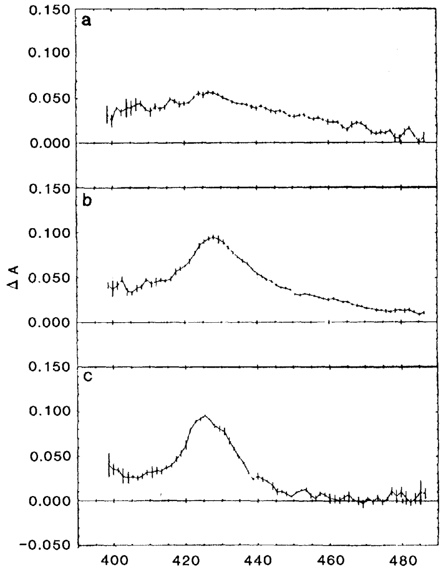

Fig. 6 (left). Streak camera records of the picosecond time emission decay of bromonaphthalenes in hexane at 20°C resulting from excitation by a 265-nm, 10-psec pulse. Fluorescence was recorded between 310 and 550 nm. Plots of emission intensity versus time are shown for (a) 1-bromonaphthalene, $\tau_f \approx 75 \pm 10$ psec; (b) 1-bromo-2-methylnaphthalene, $\tau_f \approx 72 \pm 10$ psec; (c) 1-bromo-4-methylnaphthalene $\tau_f = 80 \pm 10$ psec; and (d) 2-bromonaphthalene, $\tau_f = 150 \pm 10$ psec. Fig. 7 (right). Transient picosecond absorption spectra of 1-bromonaphthalene in hexane at 20°C on excitation with a 265-nm picosecond pulse; spectra were recorded at (a) 25 psec, (b) 100 psec, and (c) 500 psec after excitation.

Results and Discussion

The haloaromatics we have used are of the highest purity commercially obtainable, 99+ percent, and are further purified by zone refining. It is interesting to note, however, that even a large amount of impurities (5 percent) would not influence the picosecond kinetic data to any appreciable degree because the decay lifetimes are orders of magnitude shorter than the collisional frequency necessary for energy transfer to small quantities of homogeneously dispersed impurities. It was observed, for example, that reagent-grade 2-chloronaphthalene exhibited the same kinetics as the zone-refined sample. Impurities with time constants $t > 1$ nsec were detected in five samples—4-bromobiphenyl, 1-bromonaphthalene, 1-bromo-2-methylnaphthalene, and 2-bromonaphthalene, and 9-iodoanthracene—but the fluorescence intensity was less than 6 percent at time zero; an exception was a fluorescing impurity in 9-bromoanthracene, which showed a continuous-wave fluorescence of about 12 percent.

Spectrophotometric-grade hexane was further purified by passing it through a column of activated alumina. After this treatment no significant fluorescence was recorded from the hexane solvent or the quartz cells. All experiments, except when otherwise stated, were carried out at 20° ± 1°C. Fluorescence spectra were measured from 310 to ~ 610 nm. The excitation wavelength, 266 or 355 nm, was eliminated by use of Schott WG5 or Hoya L-37 colored glass filters. Picosecond transient absorption spectra were obtained by excitation of the haloaromatics with a 266-nm pulse generated by a quadrupled 1060-nm Nd^{3+}/YAG pulse.

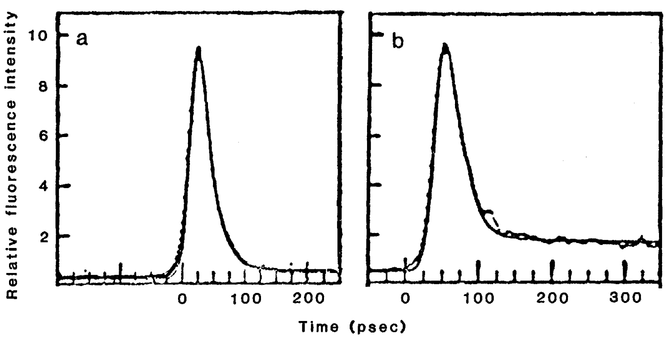

Fig. 8 Fluroescence decay of 2-iodo- and 9-iodoanthracene in hexane at 20°C after excitation with a 265- or 355-nm, 10-psec pulse. Relative fluorescence intensity versus time for: (a) 2-iodoanthracene, 310 nm < λ_f < 550 nm, $\tau_f \approx 14$ psec, and (b) 9-iodoanthracene, 310 nm < λ_f < 550 nm; $\tau_{short} \approx 3.3$ nsec.

The absorption spectra shown were recorded at time intervals from $t = 0$ to $t = 25$, 100, and 500 psec after excitation in the wavelength range 380 to 550 nm. These ranges are sufficient to cover the time constant of singlet decay and triplet or radical formation and the absorption region for $S_n \leftarrow S_1$ and $T_n \leftarrow T_1$.

It is expected that the decay lifetimes of chloroaromatics will be longer than the corresponding values for bromo- and iodoaromatics because of the increase in intersystem crossing rate with heavier halogen substitution. That this is the case is suggested from the quantum yields for fluorescence, Φ_f, and phosphorescence (*13*), Φ_p, which are reported to be $\Phi_f \approx 0.03$, $< 10^{-2}$, and $< 10^{-2}$, and $\Phi_p \approx 0.16$, 0.14, and 0.2 for 1-chloro-, 1-bromo-, and 1-iodonaphthalene, respectively (*14*). The fluorescence decays of 1-chloro- and 2-chloronaphthalene in hexane, excited by a 226-nm pulse to the first excited singlet state with an excess vibronic energy of ~ 6300 cm^{-1}, are found to be 2.4 and 3.3 nsec (*9*). It is evident, in view of the short fluorescence lifetime and low Φ_f; that most energy dissipation from the singlet state proceeds through nonradiative channels. In order to ascertain the kinetic pathway—that is, the state that couples strongly to the singlet—and establish where the energy is channeled, transient absorption spectra between 400 and 480 nm were recorded and are shown for 1-chloronaphthalene in Fig. 5 for 25, 100, and 500 psec after excitation. These spectra exhibit the expected diffuse band structure characteristic of excited singlet-singlet ($S_1 \leftarrow S_n$), transitions of large fused aromatics in solution.

In contrast, the transient absorption and emission spectra of 1-bromonaphthalene display a change in both lifetime and structure in the range 0 to 500 psec, compared to 1- and 2-chloronaphthalene. The emission spectra of spectra of 1-bromonaphthalene, shown in Fig. 6a, were obtained from molecules excited ~ 6400 cm^{-1} above the lowest vibrational level of S_1. Emission from the upper vibrational levels of S_1 was not observed, suggesting that the radiationless decay to $\nu = 0$ takes less than 5 psec. The relaxed fluorescence decay time shown in Fig. 6a is 75 ± 10 psec, which is about 30 times shorter than that of the corresponding chloro derivative. Substitution of a methyl group in the 2 or 4 position of 1-chloronaphthalene does not have any appreciable effect on the relaxation process (Fig. 6, b and c). However, substitution by bromine in the 2 position (2-bromonaphthalene) causes the lifetime to increase by a factor of 2, to 150 psec (Fig. 6d). In contrast, when the halogen is attached to the methyl group (1-chloromethyl), the lifetime of the emission becomes shorter by a factor of about 5, being 450 psec for 1-chloromethyl- compared to 2.4 nsec for 1-chloronaphthalene. Similarly, in the case of 1-bromomethylnaphthalene, we failed to observe measurable fluorescence intensity, probably because its lifetime became much shorter than 5 psec. The importance of combining transient absorption with fluorescence for unambiguous identification of the states involved and the mechanism is illustrated in Fig. 7, where transient absorption spectra of 1-bromonaphthalene between 400 and 480 nm are displayed at 25, 100, and 500 psec after excitation. The diffuse band spectrum of Fig. 7a is very similar to the $S_n \leftarrow S_1$ spectrum of chloronaphthalene. At 100 psec after excitation the spectrum (Fig. 7b) is transformed, displays a distinct peak at 425 to 430 nm and relatively low intensities at longer wavelengths, but still maintains some characteristics of the singlet-singlet absorption of the 25-psec spectrum (Fig. 7a). Close examination shows that the 100-psec spectrum (Fig. 7b) is a superposition of the 25- and 500-psec spectra (Fig. 7c). The 500-psec spectrum displays a strong 425-nm band and practically no intensity at the longer wavelengths. We believe that Fig. 7c shows the spectrum of $T_n \leftarrow T_1$, and therefore most of the excited singlet-state population has crossed over to the triplet state.

Table 1. Fluorescence lifetimes of halonaphthalenes and haloanthracenes in hexane at room temperature (~ 20°C).

Sample	λ (nm)	τ_f (psec)
4,4-Dibromobiphenyl	265	30
4-Bromobiphenyl	265	35
1-Bromonaphthalene	265	75
1-Bromo-4-methylnaphthalene	265	80
1-Bromo-2-methylnaphthalene	265	72
2-Bromonaphthalene	265	150
1-Chloromethylnaphthalene	265	490
2-Bromomethylnaphthalene	265	N.D.*
1-Chloronaphthalene	265	2400
2-Chloronaphthalene (zone refined, > 99 percent pure)	265	3300
2-Chloronaphthalene	265	3500
9-Bromoanthracene	355	100
9,10-Dibromoanthracene	355	1300
2-Iodoanthracene	265	14
9-Iodoanthracene	265	35
2-Iodoanthracene	355	17
9-Iodoanthracene	355	55

*Not detected.

The absorbance change at any particular wavelength and time, $\Delta A(\lambda,t)$, is given by

$$\Delta A(\lambda,t) = A(\lambda)e^{-t/\tau_f} + B(\lambda)\,(e^{-t/\tau_p} - e^{-t/\tau_f})$$

where τ_f and τ_p are the fluorescence and phosphorescence lifetimes, respectively, and $A(\lambda)$ and $B(\lambda)$ are the relative amplitudes at a particular wavelength of the $S_1 \rightarrow S_n$ and $T_1 \rightarrow T_n$ transitions times their concentrations and path lengths.

The fact that the emission decay of the first excited singlet state and the rise time of the triplet state both occur with a lifetime of 75 ± 10 psec strongly suggests that bromonaphthalene, under the conditions of the experiment, dissociates from the triplet state. The higher rate for bromo- versus chloronaphthalene found in both absorption and emission kinetics provides an additional strong indication that intersystem crossing ($S_1 \rightarrow T$) is the dominant process (*2*, *14*). Further illustration of the techniques and support for the dissociation model proposed is provided by the iodoaryls. Under the same excitation conditions, the emission lifetime of 2-iodoanthracene is found to be 14 psec (Fig. 8). Similar short emission lifetimes for other halogenated aromatics are shown in Table 1. The transient absorption spectrum of 2-iodoanthracene (Fig. 9a) does not show a strong singlet-singlet absorption at 25 psec after excitation. This indicates that intersystem crossing and partial dissociation from S_1 take place within the first 20 psec after excitation (*15*). The transient spectra recorded at the later times (Fig. 9, b and c) exhibit the same band structure as the $T_n \leftarrow T_1$ spectra of iodoanthracene recorded previously by Morgante and Stuve (*16*). More evidence for the mechanism of dissociation and radical formation is also provided by study of the C–X bonds through picosecond Raman scattering and detection of the emission spectra and kinetics of the radical formed.

Recently, Kelley and Rentzepis (*17*) studied the emission spectra and formation kinetics of aromatic radicals formed by the photodissociation of haloaromatics. Because the concentration of radicals formed by picosecond photodissociation is small, and in some cases the absorption cross section is low, they used a two-color picosecond excitation technique to induce fluorescence of the radical. The first color pulse is the one described above, which excites the parent haloaromatic to S_1. The second is a longer wavelength which is sufficient to excite the radical usually formed in the ground state but not sufficient to excite the parent. By delaying the longer wavelength pulse and monitoring the time of appearance of radical emission, it was possible to directly measure the dissociation lifetime or radical formation time very accurately. This technique is illustrated for the dissociation of 2-bromomethylnaphthalene. When this molecule was excited with a 266-nm pulse, no measurable fluorescence was observed for either parent or radical (see Table 1); however, when it was simultaneously excited with 355- and 266-nm pulses, fluorescence was recorded with the spectrum shown in Fig. 10 and the formation and decay lifetime shown in Fig. 11. When the 355-nm (radical-exciting) pulse preceded the 266-nm (parent-exciting) pulse no emission was detected. However, when the 355-nm pulse followed the 266-nm one by as much as 400 psec (interval of time tested) the kinetics and spectra remained identical.

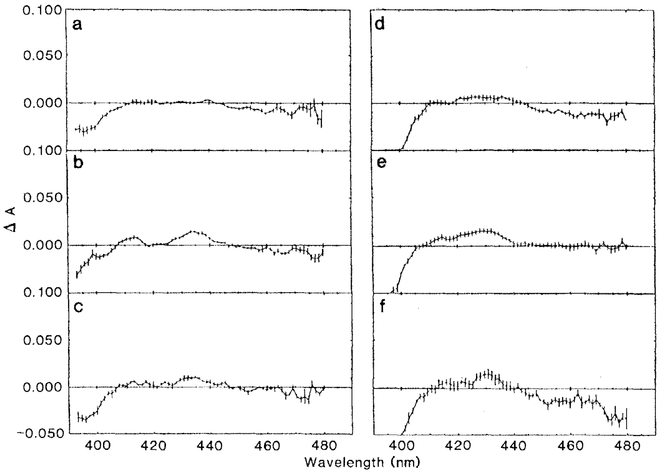

Fig. 9. Transient absorption spectra at 20°C of (a to c) 2-iodoanthracene in hexane and (d to f) 9-iodoanthracene in hexane.

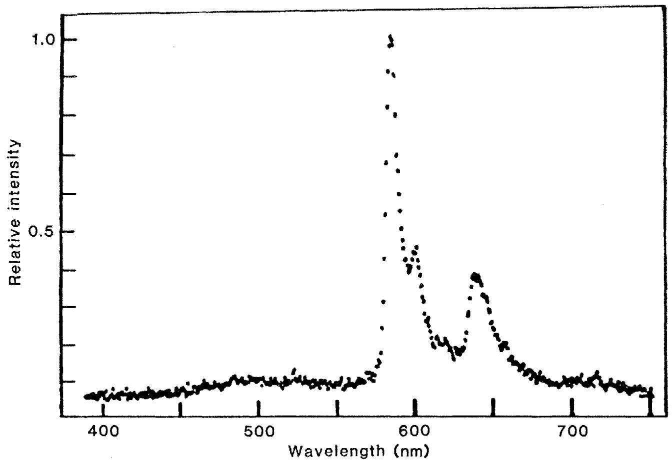

Fig. 10. Emission spectrum of the naphthyl radical.

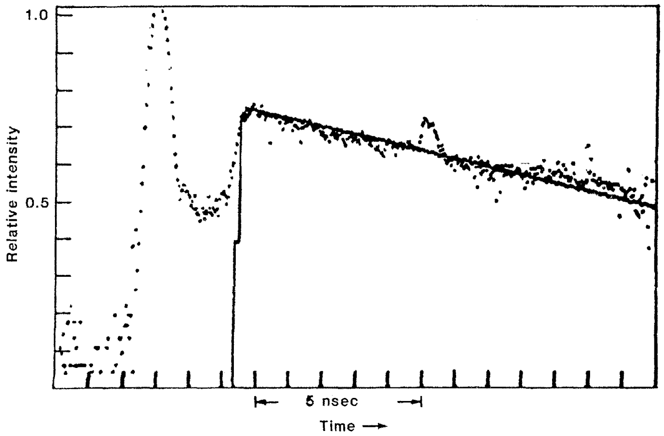

Fig. 11. Emission kinetics of the naphthyl radical. The initial segment of the curve formed by the experimental points is due to a 530-nm trigger pulse; the subsequent signal shown by the continuous curve depicts the kinetics of formation and decay of the naphthyl radical.

The fact that the radical emission appears immediately after the excitation of the parent shows that the dissociation process is completed within 15 psec and occurs from the singlet state when X = Br or Cl. This dissociation lifetime is in agreement with the absence of emission from the parent molecule (Table 1). In addition, the spectrum of the 355-nm induced emission shown in Fig. 11 corresponds to the naphthyl radical emission. Other radical species have been identified by similar means by photodissociation of several haloaromatics and other species including diazene, where nitrogen is cleaved, resulting in a biradical whose identity and kinetics have been studied extensively by Kelley and Rentzepis (*17*).

In another study, Kelley *et al.* (*18*) investigated the photolytic dissociation of diazene to generate a biradical by cleavage of the nitrogen bond and completely identified the transient fluorescence spectrum; the predissociation singlet lifetime was found to be ~ 38 psec in addition to the long-lived 280-psec biradical emission. The picosecond data for the compounds discussed, and for several others presented in Table 1, show the progress that has been made in picosecond spectroscopy. It is possible not only to monitor and directly record simple relaxation processes but also to follow, with high time resolution, the course of more complex photochemical reactions from the initial excitation through the intermediate states or transient species to radical formation and identification and, if need be, to recombination or generation of new chemical species. In addition, the methods used promise to provide insight into the mechanisms of radical and ionic polymerization and, through the ability to identify transient states and their decay channels and lifetimes, to lead toward the generation of chemical species with novel properties.

References and Notes

1. A. Friedman and R. Bersohn, *J. Am. Chem. Soc.* **100**, 4116 (1978).
2. R. L. Pineault, C. G. Morgante, W. S. Struve, *J. Photochem.* **17**, 435 (1981).
3. Y. B. Band and K. F. Freed, *J. Chem. Phys.* **64**, 4324 (1976).
4. M. Dzwonic, S. Yang, R. Bersohn, *ibid.* **61**, 4408 (1974).
5. P. M. Rentzepis, *Science* **202**, 174 (1978).
6. C. G. Morgante and W. S. Struve, *Chem. Phys. Lett.* **68**, 272 (1982).
7. G. D. Gillispie and E. C. Lim, *J. Chem. Phys.* **65**, 2023 (1976).
8. C. Crentz, M. Chou, T. L. Netzel, *J. Am. Chem. Soc.* **103**, 1309 (1980).
9. D. Huppert, S. D. Rand, A. H. Reynolds, P. M. Rentzepis, *J. Chem. Phys.* **77**, 1214 (1982).
10. P. F. Barbara, L. E. Brus, P. M. Rentzepis, *Chem. Phys. Lett.* **69**, 447 (1980).
11. D. Huppert, J. Jortner, P. M. Rentzepis, *Isr. J. Chem.* **76**, 182 (1978).
12. P. M. Rentzepis and D. C. Douglass, *Nature (London)* **293**, 165 (1980); D. F. Kelley and P. M. Rentzepis, *Chem. Phys. Lett.* **85** (No. 1) (1982).
13. C. J. Calvert and J. Pitts, *Photochemistry* (Wiley, New York, 1966).
14. A. Friedman, S. C. Yang, M. Kuwasaki, R. Bersohn, *J. Chem. Phys.* **72**, 2115 (1980).
15. S. C. Yams, A. Friedman, M. Kuwasaki, R. Bersohn, *ibid.*, p. 4058.
16. C. G. Morgante and W. S. Struve, *Chem. Phys. Lett.* **68**, 277 (1979).
17. D. F. Kelley and P. M. Rentzepis, *J. Am. Chem. Soc.*, in press.
18. D. F. Kelley, M. R. Mazur, J. A. Berson, P. M. Rentzepis, *ibid.* **104**, 3764 (1982).
19. Discussions and collaborations with D. C. Douglass have been invaluable assets in this work. Most of the research work presented in this article was performed with P. F. Barbara (University of Minnesota), D. Huppert (University of Tel Aviv), A. H. Reynolds, and S. D. Rand.

Japanese Supercomputer Technology

B. L. Buzbee, R. H. Ewald, W. J. Worlton

In February 1982, computer scientists from the Los Alamos National Laboratory and Lawrence Livermore National Laboratory (*1*) visited several Japanese computer manufacturers (*2*). The purpose of these visits was to assess the state of the art of Japanese supercomputer technology and to advise Japanese computer vendors of the needs of the U.S. Department of Energy (DOE) for more powerful supercomputers.

The Japanese foresee a domestic need for large-scale computing capabilities for nuclear fusion, image analysis for the Earth Resources Satellite, meteorological forecast, electrical power system analysis (power flow, stability, optimization), structural and thermal analysis of satellites, and very large scale integrated circuit design and simulation. To meet this need, Japan has launched an ambitious program to advance supercomputer technology.

Japanese National Projects

In discussions with H. Kashiwagi of the Electro-Technical Laboratory (a government-funded organization, something like a U.S. national laboratory) we learned that the Japanese are using the concept of national projects to advance the development of supercomputers. Eight national projects in different areas have already been completed (*3*), and nine were still in progress at the end of 1981 (see Table 1). National projects relevant to computers include the National Superspeed Computer Project, the Fifth-Generation Computer Project, and the Functional Device Project. The criteria used by the Japanese for selecting national projects for research and development are as follows.

- The technology is urgently required for upgrading national industrial standards, promoting efficient utilization of natural resources, and preventing industrial pollution.
- The technology is expected to make a great impact on the progress of mining and manufacturing industries.
- The technology cannot be undertaken by private firms because of high risk, huge investment requirements, long-term programming, or absence of profit motives.
- The technology has clearly specified targets and well-examined attainment prospects.
- The project will be carried out in cooperation with universities and industry.

In this article we focus most of our discussion on the National Superspeed Computer Project. We also comment on the Fifth-Generation Computer Project, and describe some of the implications of these projects for the United States.

National Superspeed Computer Project

The six major Japanese computer vendors (Fujitsu, Hitachi, Nippon Electric Company, Mitsubishi, Oki, and Toshiba), in cooperation with the Electro-Technical Laboratory, have joined in the National Superspeed Computer Project to develop a computer more powerful than any now available. The joint effort is organized as the Scientific Computer Research Association.

Funding and duration. The superspeed computer project is funded by the Ministry of International Technology and Industry (MITI), with additional support from each of the six vendors. MITI funding for fiscal year 1982 will be 800 million yen (about $3.8 million). Fifteen percent of the funding for this project will go to the Electro-Technical Laboratory, and the other 85 percent will go to the other participants. Since the salaries of the researchers at the Electro-Technical Laboratory are already paid by the government, the funding for the superspeed computer project is larger than it may appear. Also, this funding may provide up to twice as much manpower in Japan as in the United States because salaries are lower there. Total funding for this project is expected to be about $200 million.

The National Superspeed Computer

R. H. Ewald is division leader and B. L. Buzbee and W. J. Worlton are assistant division leaders of the Computing Division, Los Alamos National Laboratory, Los Alamos, New Mexico 87545.